SSRG International Journal of Civil Engineering
ISSN: 2348-8352/ https://doi.org/10.14445/23488352/IJCE-V13I8P128

Volume 13 Issue 8, 469-486, August 2026
© 2026 Seventh Sense Research Group®

Original Article

Comparative Assessment of Machine Learning Models for Predicting Seismic Displacements of Concrete Gravity Dams

Mohammed Elmorsli[1], Mouna El Mkhalet[2], Nouzha Lamdouar[3]

[1,2,3]*Civil Engineering and Construction Structure GCC Laboratory, Mohammadia School of Engineers, Mohammed V University, Rabat, Morocco.*

[1]*Corresponding Author : elmorslimohammedem@gmail.com*

Received: 25 December 2025 Revised: 08 July 2026 Accepted: 12 August 2026 Published: 31 August 2026

Abstract - *Concrete gravity dams constitute critical hydraulic infrastructures whose seismic response is crucial for maintaining structural stability and safety. The present study investigates the performance of three machine learning algorithms, namely Multilayer Perceptron (MLP), Support Vector Regression (SVR), and Extreme Gradient Boosting (XGBoost), for predicting the maximum seismic displacement of concrete gravity dams within a Single-Degree-Of-Freedom (SDOF)-based seismic reliability framework. A dataset comprising 304 samples was generated through parametric finite element simulations by varying the principal geometric and material properties of the dam system. The predictive performance of the models was evaluated using six-fold cross-validation based on the coefficient of determination (R^2), Root Mean Square Error (RMSE), and Mean Absolute Error (MAE). Among the evaluated algorithms, MLP achieved the highest prediction accuracy, whereas XGBoost demonstrated comparable performance. SHAP and perturbation-based sensitivity analyses consistently identified dam height as the most influential parameter governing the predicted seismic displacement. The proposed framework provides an efficient and interpretable approach for rapid seismic displacement prediction and seismic reliability assessment of concrete gravity dams.*

Keywords - *Concrete Gravity Dams, Multilayer Perceptron, Seismic Displacements, Support Vector Regressions, Xgboost Models.*

1. Introduction

Concrete gravity dams constitute strategical hydraulic structures that play a crucial role in irrigation, water resource supply, hydroelectric energy production, and flood risk management [1]. Among civil engineering structures, dams are highly susceptible to deformation caused by hydrostatic loading, geotechnical instabilities and seismic activity [2]. Therefore, ensuring dam safety is a critical requirement for infrastructure asset management [3]. It is essential not only for structural stability but also directly impacts the safety of human lives and property [4].

In this regard, seismic events present significant challenges for concrete gravity dams, due to the highly coupled interaction between seismic loading, hydrodynamic pressures, and dam structural properties [5]. Therefore, dam deformation serves as a critical visual indicator for evaluating the safety and the structural performance of concrete gravity dams subjected to complex loading conditions [6].

Dam deformation is influenced by multiple interacting factors, including water level, sediment accumulation, thermal variations and material properties [3]. Consequently, implementing an accurate deformation prediction model is crucial for ensuring safety monitoring and maintaining operational performance of concrete gravity dams [7].

In recent years, artificial intelligence methods have become increasingly adopted across multiple engineering disciplines [8]. Indeed, machine learning models such as the Artificial Neural Network (ANN), the Support Vector Regression (SVR) algorithm, and the Extreme Gradient Boosting (XGBoost) algorithm have been successfully applied for predicting concrete dam deformation [6].

Unlike conventional statistical techniques, machine learning models can capture complex and nonlinear relationships directly from observed data to improve prediction performance [7].

Moreover, the integration of artificial intelligence-based methods in dam deformation prediction have demonstrated several advantages, including high predictive accuracy and low computational cost [9].

2. Machine Learning Applications in Civil Engineering

2.1. Application of Multilayer Perceptron

The concept of Artificial Neural Networks (ANNs) was first introduced in 1943 through the collaborative research between Warren McCulloch and Walter Pitts. [10] An ANN represents a computational model developed to simulate the structural and functional principles of the human brain's neural networks [11].

Furthermore, ANNs constitute the essential core of deep learning models, providing the versatility, robustness, and scalability that enable them to handle complex and large machine-learning tasks [10]. As a type of artificial neural networks, the Multilayer Perceptron (MLP) represents one of the most widely employed models in deep learning and machine learning [12]. Compared to other machine learning algorithms, MLPs demonstrate greater ability in capturing complex nonlinear interactions between inputs and outputs, especially in the context of high-dimensional dataset [13].

Several studies have explored the application of the multilayer perceptron model in structural and seismic engineering. Indeed, according to Kim et al. (2024), MLP networks successfully predicted the properties of soil consolidation related to geotechnical engineering problems [14].

Furthermore, in their study, Guzmán Sejas et al. (2025) employed MLP-based models to predict the natural frequencies of a concrete arch dam [15]. Moreover, Alouan et al. (2025) applied MLP models to predict concrete compressive strength and demonstrated their robustness in predictive effectiveness [16].

2.2. Application of Support Vector Machine

Support Vector Machine (SVM) constitute a supervised learning algorithm widely used for handling both classification and regression problems [17]. Introduced by Vapnik, SVM models are based on the principle of separating observations through the creation of hyperplanes that maximize the distance between the upper and lower boundaries defined by the dataset [18]. The SVM algorithm was initially developed for binary classification tasks, then extended to solve multi-class problems as well [19].

Regarding the application of SVM in civil engineering, in the study conducted by Harirchian et al. (2020), SVM was used to evaluate the seismic safety of existing buildings based on structural indicators [20].

Similarly, the findings of Shao et al. (2023) demonstrated that SVM stands out as one of the top machine learning algorithms in geotechnical engineering, surpassing ANN and decision trees models for rock classification and deformation prediction tasks [21]. Furthermore, according to Anuragi (2024), the SVM method effectively captures complex geotechnical datasets through kernel functions and optimized hyperparameters, achieving high predictive performance for foundations and soil–structure interactions [22].

2.3. Application of Extreme Gradient Boosting

Decision-tree-based machine learning algorithms have progressively become widely recognized as fundamental instruments to capture complex non-linear relationship in hydraulic engineering applications, particularly for the prediction of dam displacements under diverse loading conditions [23].

The XGBoost algorithm is a widely recognized technique in the gradient boosting family, which performs effectively for classification and regression problems [24]. In 2016, Chen and Guestrin introduced the XGBoost algorithm, built upon the Gradient Boosting Decision Trees (GBDT) architecture, has gained broad recognition due to its remarkable achievements in Kaggle's ML competitions [25]. The algorithm employs a supervised learning model through a gradient boosting framework that constructs an ensemble of multiple decision trees [26].

As for the application of XGBoost, in applied engineering, XGBoost has demonstrated a stable predictive capability, comparable to deep neural networks [27]. Furthermore, in pavement structural assessment, several comparative studies have revealed that XGBoost achieves significant predictive performance [28].

Moreover, combining XGBoost with multiple optimization techniques has achieved significant performance in cementitious material research, leading to superior strength prediction accuracy for fiber-reinforced cemented backfills [29]. In geopolymer concrete research, XGBoost-based hybrid models have demonstrated a significant increase in the precision of strength prediction [30]. Similarly, in the context of green building projects, XGBoost has effectively provided more reliability in cost estimations compared with traditional methods [31].

Moreover, although existing studies have explored machine learning applications for seismic dam assessment, systematic comparative evaluations of multiple algorithms for dams' displacement prediction to identify the most suitable for each structural configuration remain limited. Table 1 provides an overview of previous studies investigating the application of machine learning methods to seismic dam engineering problems. As summarized in this Table, previous researches have mostly focused on operational dam displacement monitoring through individual machine learning models or advanced deep learning architectures. Consequently, Comparative evaluations of computationally efficient machine learning algorithms for seismic displacement prediction of concrete gravity dams remain limited.

Table 1. Overview of recent machine learning applications for concrete dam displacement prediction

Reference	Research Objective	Prédictive model	Key Limitations
Qiubing Ren et al. (2022) [32]	Multi-point prediction of concrete dam displacement.	SVR	No comparison with alternative ML algorithms to identify the most appropriate predictive approach
Guzmán Sejas et al. (2025) [15]	Prediction of the dynamic behavior of concrete dams using monitoring data.	MLP & Statistical Models	Limited to the MLP & Statistical Models without assessing other machine learning algorithms to determine the most suitable predictive model.
Chongshi Gu et al. (2023) [33]	Prediction of concrete gravity dam displacement in severely cold regions.	SVR	Limited to displacement health monitoring models, without a comparative evaluation with other machine learning models.
Bo Xu et al. (2025) [34]	Prediction of concrete dam displacement considering lag effects and cracks.	XGBoost	Focused on deep learning architectures (XGBoost) without benchmarking alternative standalone machine learning algorithms to identify the most suitable predictive model

To address the identified research gaps, the present study aims to comparatively evaluate the performance of different machine learning models in predicting seismic displacement of concrete gravity dams generated from finite element simulation data. In this context, machine learning models based on Multilayer Perceptron (MLP), Support Vector Regression (SVR), and Extreme Gradient Boosting (XGBoost) are developed and comparatively evaluated to identify the most suitable model for seismic displacement prediction. Accordingly, the main objectives of this study are as follows:

- To generate a finite element simulation dataset for concrete gravity dams under combined seismic and hydrostatic loading conditions.
- To implement three machine learning models, namely MLP, SVR, and XGBoost, for predicting concrete gravity dam displacement.
- To identify the optimal machine learning model through a comparative assessment of predictive accuracy and robustness.

3. Materials and Methods

The present research focuses on eight concrete gravity dams, selected to represent a range of geometrical characteristics, mechanical properties and loading conditions. Initially, structural performance during hydrostatic and seismic excitations was evaluated using the maximum horizontal displacement. Then, the seismic reliability of each dam was evaluated through a Monte-Carlo Single Degree of Freedom (SDOF) model. This method is widely used to evaluate structural behavior under dynamic excitations. The response of a SDOF system can be expressed by the following linear differential equation:

$$\mathrm{m}\ddot{u}(t) + \mathrm{c}\dot{u}(t) + \mathrm{k}u(t) = -\,\mathrm{m}\ddot{u}_g(t) \qquad (13)$$

where:

- m: the equivalent mass (kg)
- c: the damping coefficient (N·s/m)
- k: the system stiffness (N/m)
- $u(t)$: the relative displacement (m)
- $\ddot{u}_g(t)$: the ground acceleration (m/s²)

The admissible horizontal displacement under hydrostatic and seismic loads was defined as a ratio of the dam height. Each dam was modeled as simplified SDOF systems to efficiently capture the dominant horizontal dynamic behaviour. Table 2 presents the main SDOF model parameters.

Table 2. Essential SDOF model parameters

Parameter	Symbol	Unite	Adopted range / value
Dam height	H	m	29 – 67
Equivalent mass	M	Kg	$3\text{x}10^6$ – $8\text{x}10^6$
Natural period	$\mathrm{T_n}$	s	0.3 – 1.5
Damping ratio	ξ	–	0.03 – 0.07
Peak ground acceleration	PGA	m/s²	1.5 – 4
Allowable displacement	$\mathrm{u_{allow}}$	m	H / 700

Monte-Carlo simulations were applied with numerous random variations seismic acceleration scenarios ranging from 0.15 g to 0.4 g based on the number of Monte Carlo simulations N=1000. This method yielded the probability of failure when surpassing the admissible displacement and the reliability index for each dam.

Subsequently, a dataset comprising 304 observations was generated through finite element simulation. The input dataset included geometric characteristics, concrete material properties, and loading conditions, while the corresponding maximum horizontal displacement serving as the target output. Table 3 summarizes the descriptive statistics of the dataset used in this study.

Table 3. Descriptive statistics of the input and output variables used in this study

Variable	Min	Max	Mean
Dam Height (m)	29	67	52.75
Dam Length (m)	120	280	225.00
Density (kg/m³)	2300	3500	2621.05
Elastic Modulus (GPa)	25	50	35.05
Maximum Displacement (m)	0.003921	0.033825	0.014421

As illustrated in figure 1 and 2, the applied loading to each dam included the self-weight of the structure, hydrostatic pressure, and horizontal seismic acceleration.

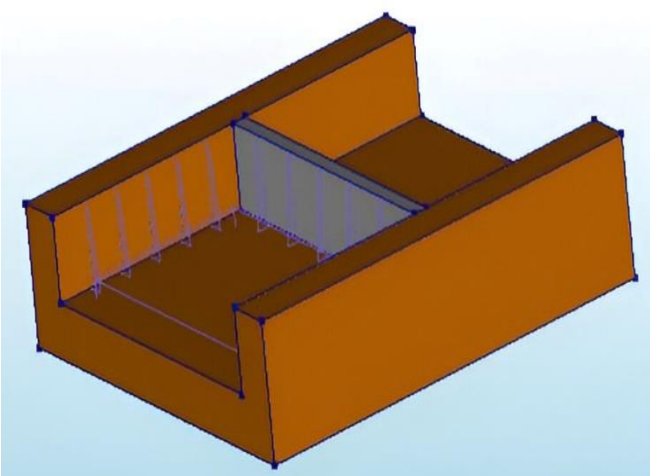

Fig. 1 Simplified dam model under hydrostatic and seismic loads

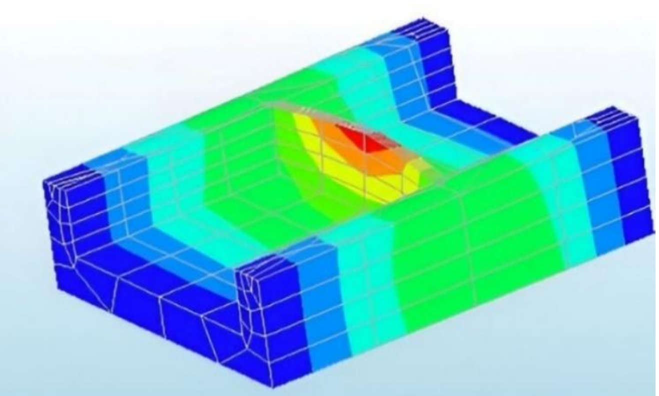

Fig. 2 Distribution of horizontal displacement response under the applied loads

In the next step, dynamic analyses were conducted under multiple acceleration scenarios to represent a wide range of seismic intensity. The maximum horizontal displacement at the dam crest was extracted from each simulation and used as the target output for training, validating, and comparing the artificial intelligence models.

Moreover, the dataset was normalized and assessed using a six-fold cross-validation to ensure robust evaluation of machine learning models in the prediction of maximum horizontal displacement. The predictive performances of the proposed models, namely MLP, SVR, and XGBoost, were comparatively evaluated through performance metrics such as the Root Mean Squared Error (RMSE), Mean Absolute Error (MAE), and the coefficient of determination (R^2).

3.1. Multilayer Perceptron Model

Structurally, the MLP architecture is composed of three principal layers: an input layer, one or more hidden layers, and an output layer [11]. In these structural configurations, every node of one layer is linked to all nodes of the adjacent layers, thereby forming a fully connected network [12]. Within an MLP architecture, the number of neurons in the input layer corresponds to the number of independent features, the hidden layers function as processing units, and the output layer executes prediction and classification tasks [35]. Figure 3 illustrates the multilayer perceptron structure.

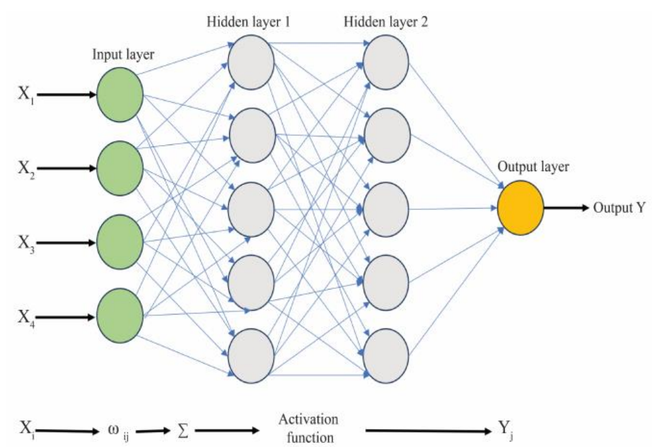

Fig. 3 Illustration of the MLP neural network structure

During the learning process, every connection in the network is assigned a weight w; and during supervised learning, the neuron generates its output through an activation function applied to the weighted sum of inputs, adjusted with a bias term [36], as expressed in Equation (1).

$$Sum_j = \sum_{i=1}^{n} w_{ij} * x_i + b_j \tag{1}$$

Here, w_{ij} refers to the connection weight linking input neuron i and hidden neuron j, x_i indicates input features or preceding-layer outputs, and bj represents the associated bias term of the hidden neuron [15].

$$y_j = f\ (Sum_j) \quad (2)$$

y_j represents the final output value produced by neuron j, while f corresponding to the sigmoid activation function [11].

Its computation is presented in Equation. (3)

$$f\ (Sum_j)\ = \frac{1}{1+e^{Sum_j}} \quad (3)$$

The activation function introduces nonlinearity into the neural network, thereby enables it to model complex data distributions and to execute regression tasks [39]. The principal activation functions are types are as follows:

$$\text{ReLU}\ (x) = \max\ (0, x) \quad (4)$$

$$\text{Sigmoid}\ (x) = \frac{1}{1+\ e^{-x}} \quad (5)$$

$$\tanh\ (x) = \frac{1-\ e^{-2x}}{1+\ e^{-2x}} \quad (6)$$

Every node propagates its activation only in the forward direction, transmitting its output to the next layer of the network [12]. In the training phase, the network weights are iteratively updated to minimize the loss function, thereby decreasing the quadratic error between predicted and actual outputs. This iterative process continues until the network achieves a minimum value through error backpropagation [36].

Finally, a hyperparameter optimization procedure based on Grid Search and six-fold cross-validation was performed to identify the optimal MLP architecture. Indeed, different combinations of hidden layer structures, activation functions, learning rates, and regularization parameters were evaluated to achieve the optimal configuration according to the highest mean cross-validation R^2 achieved through the Grid Search.

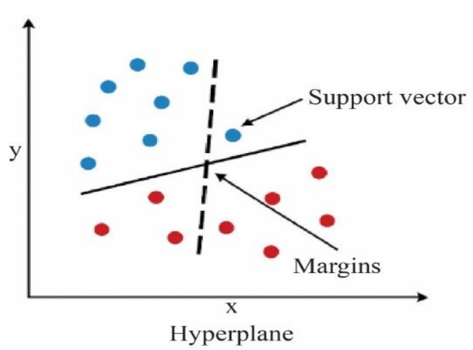

Fig. 4 Illustration of a binary classification case solved by SVM model

3.2. Support Vector Machine Model

The fundamental principle of SVM is to identify an optimal hyperplane that separates data points belonging to different classes while maximizing the margin between them [17]. The optimal hyperplane is defined by the support vectors, which are the training points closest to the decision boundary [13]. Figure 4 illustrates a simplified graphical representation of a binary classification case solved by SVM.

The kernel function is employed to generate a nonlinear hyperplane including all the set of input features in the classification process. The performance of SVM is critically influenced by the choice of kernel function and the parameter values applied as default or set values [36]. Support Vector Machines is well-suited particularly for high-dimensional feature spaces and can handle both linear and nonlinear relationships using appropriate kernel functions [37]. The separating hyperplane in the higher-dimensional transformed feature space can be mathematically expressed as:

$$\omega^T x + b = 0 \quad (7)$$

Were:

- x: the input feature vector;
- ω : the weight vector;
- b: the bias or offset term;
- $\omega^T x + b$: the signed distance of a point from the hyperplane.

The most widely used kernel functions in SVM include the linear, polynomial, Radial Basis Function (RBF), and sigmoid types [40]. These formulations are expressed in the following equations:

$$\text{Linear Kernel}:\ k\ (x_i, x_j) = {x_i}^T\ x_j \quad (8)$$

$$\text{Polynomial Kernel}: k\ (x_i, x_j) = (\gamma {x_i}^T x_j + r\ )^d \quad (9)$$

$$\text{RBF/ Gaussian Kernel}: k\ (x_i, x_j) = \exp\ (-\gamma \left\| x_i - x_j \right\|^2) \quad (10)$$

$$\text{Sigmoid Kernel}: k\ (x_i, x_j) = \tanh\ (\gamma {x_i}^T x_j + r) \quad (11)$$

Here, (x_i, x_j) correspond to the input feature vectors, k (x_i, x_j) indicates the similarity measure between x_i and x_j, d represents the degree of the polynomial, r denotes the constant term. The kernel coefficient γ is a positive parameter that affects various kernels in multiple ways. In linear kernels, it has no impact, whereas in the polynomial kernel, it serves as a scaling factor for feature interactions, enhancing the degree of nonlinearity.

For the RBF kernel, γ controls the width of the Gaussian function and regulates the influence of training data points to the decision boundary. For the sigmoid kernel, γ defines the intensity of interactions between features [39]. Figure 5 illustrates the main steps of the Support Vector Machine (SVM) algorithm.

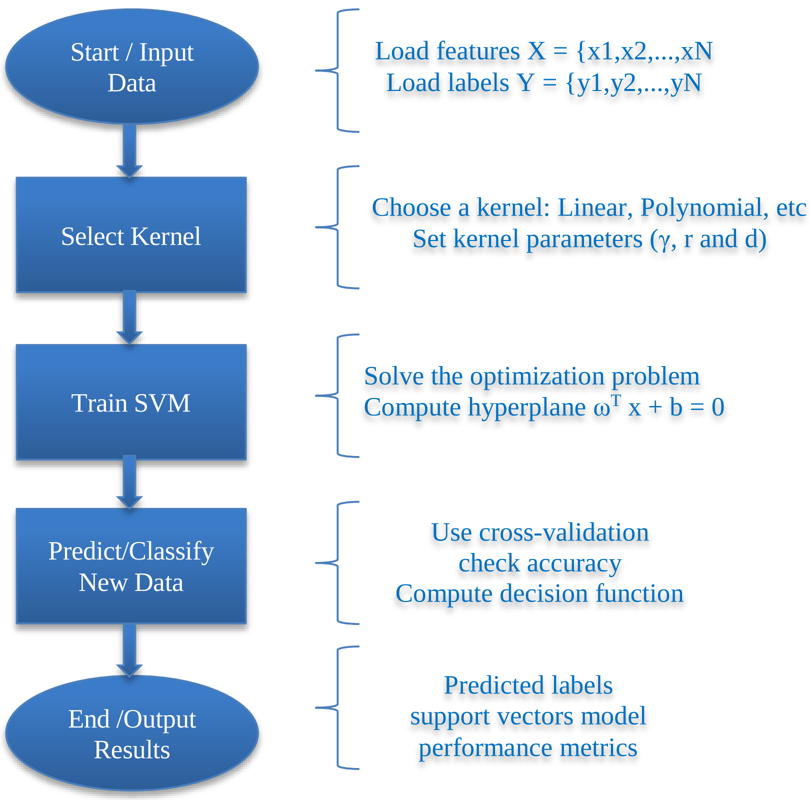

Fig. 5 Flowchart of the SVM Classification Process

In the present study, we focused on the Support Vector Regression (SVR) model, which corresponds to the regression equivalent of the Support Vector Machine (SVM). Although SVM is primarily used for classification tasks, SVR extends its same kernel and maximum-margin concepts to regression and prediction of continuous structural responses. The model establishes an optimal regression function that minimizes prediction errors and effectively captures the relationship between dam height, dam length, material density, elastic modulus, and the corresponding displacement response. Furthermore, the optimal SVR configuration was determined through a grid-search optimization procedure and subsequently evaluated using six-fold cross-validation.

3.3. Extreme Gradient Boosting Model

XGBoost applies gradient boosting to transform a set of weak learners into a strong predictive model [41]. This model is capable of automatically handling missing data, which can be advantageous for infrastructure monitoring with high levels of data absence [28]. In this sequential process, each new model learns from the residual errors of its predecessor and enhances predictive accuracy by systematically adjusting weights [28]. For a given sample (x_i,y_i), each input variable x_i contains distinct features corresponding to an output value y_i . The predicted output value $\hat{y}_i$ for the i-th input value x_i can be formulated as:

$$\hat{y}_i = \sum_{k=1}^{N} F_k(x_i) \tag{12}$$

In this formulation, N signifies the number of decision trees, while $F_K(x_i)$ corresponds to the prediction output generated by the k-th regression tree for the input x_i. The main idea is that each XGBoost computes $\hat{y}_i$ by summing the outputs of N individual decision trees results [28].

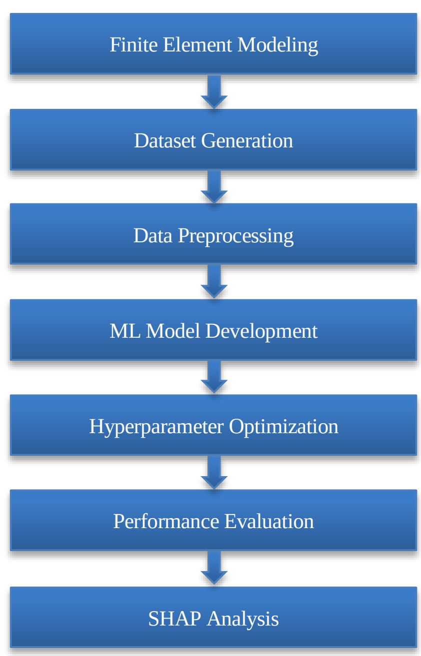

Fig. 6 Workflow of the proposed methodology

To maximize the predictive performance of the XGBoost model, a Grid Search optimization procedure combined with six-fold cross-validation was conducted. Several combinations of hyperparameters controlling the learning process and tree structure, such as the learning rate, maximum tree depth, number of estimators, subsample ratio, and column sampling ratio, were systematically evaluated to identify the optimal model configuration. The proposed methodology consists of data preparation, machine learning model development and optimization, performance evaluation, and explainability analysis, as illustrated in Figure 6.

4. Results and Discussion

4.1. Failure Reliability Results

The seismic reliability analysis was applied for eight dams through a simplified SDOF model combined with Monte Carlo simulations. Horizontal displacement was defined as the performance criterion, with an admissible limit of H/700, where H represents the dam height. Moreover, calculated displacements were compared to the admissible limit, ensuring conformity with engineering standards. Table 4 presents the obtained results.

Table 4. Seismic reliability results of the simulated dams based on a simplified SDOF model

Dam	Height H (m)	Mean Displacement (m)	Max Displacement (m)	Allowable Displacement u_{allow} (m)	Failure Probability	reliability index β
1	50	0.041027	0.053163	0.071429	0.182750	0.561045
2	64	0.055263	0.081301	0.091429	0.273618	1.124547
3	29	0.026959	0.025940	0.041429	0.107103	1.280464
4	64	0.048067	0.064351	0.091429	0.107049	1.092899
5	43	0.041617	0.042102	0.061429	0.281035	0.916682
6	67	0.054131	0.060692	0.095714	0.291473	0.885445
7	45	0.035938	0.048941	0.064286	0.210774	1.103491
8	60	0.057985	0.074555	0.085714	0.154298	0.774458

The results indicate that, for each of the studied dams, the simulated maximum displacements do not exceed the admissible limit, as illustrated for an example of Dam_2 in Figure 7. The results indicate that the probability of failure is ranged from 0.11 to 0.29 for all studied cases, corresponding to moderate reliability indices (β) ranging
from 0.56 to 1.28, reflecting an acceptable structural safety under the considered seismic loading.

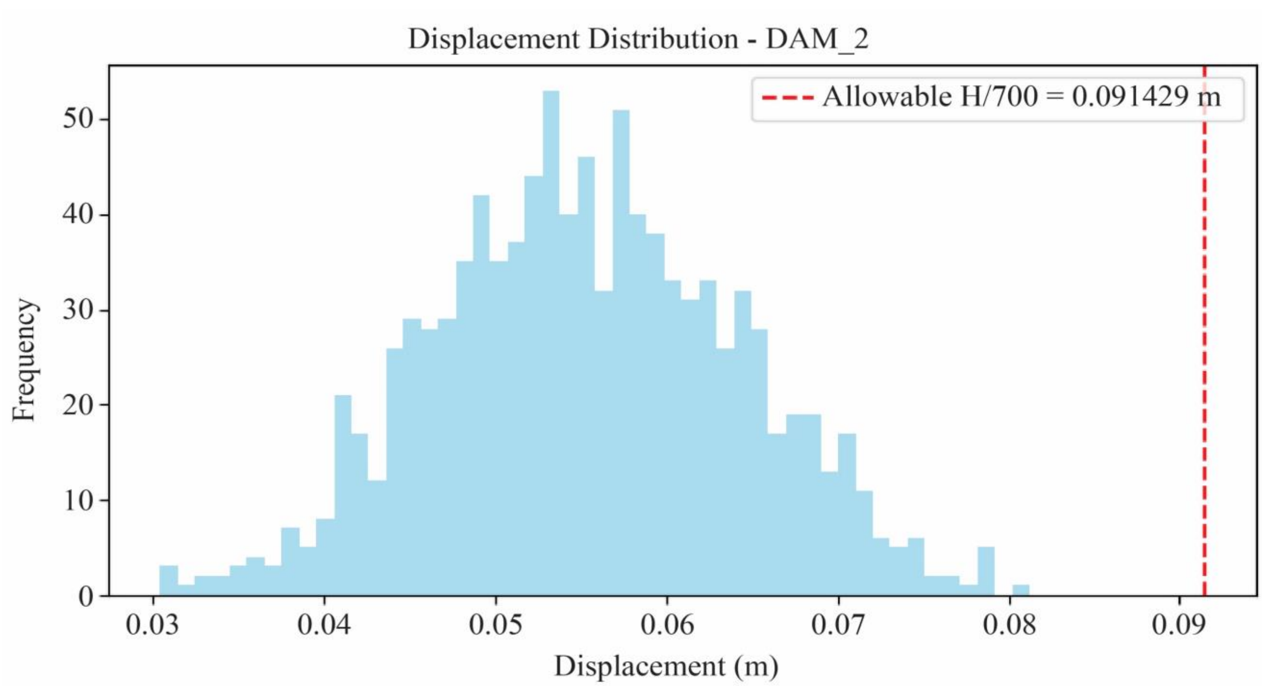

Fig. 7 Monte Carlo-Based distribution of dam 2 maximum displacements with the admissible limit.

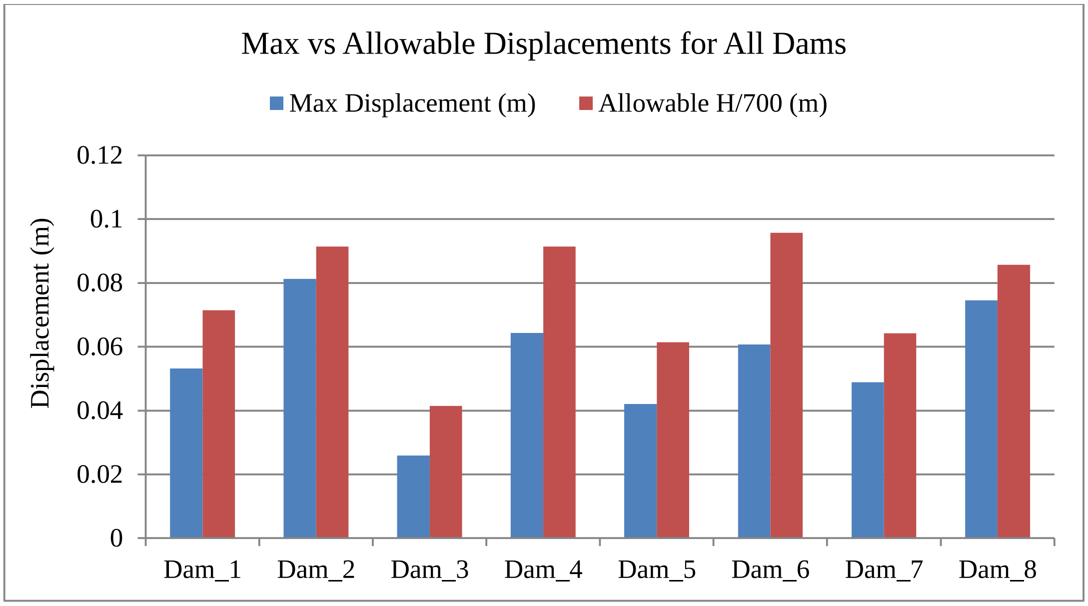

Fig. 8 Comparison between maximum seismic displacement and allowable displacement for each studied dam.

The figure 8 illustrates the comparison between the maximum seismic displacements derived from Monte Carlo simulations and the allowable displacement limits determined by the H/700 criterion for each dam, and shows that all investigated cases satisfy the adopted structural safety criterion, indicating that the considered concrete gravity dams remain within the acceptable seismic safety limits.

4.2. Multi-Layer Perceptron Model Performance

4.2.1. MPL with ReLU Activation

The MLP architecture consists of two fully connected hidden layers of 64 neurons each, with three types of activation functions. The MLP model with RELU activation reveals high predictive accuracy throughout the six-fold cross-validation, with R^2 values ranging from 0.9628 to 0.9927, demonstrating robust capture of the variance in the dataset. The Root Mean Square Error (RMSE) varies between 0.0879 and 0.1934 m, while Mean Absolute Error (MAE) ranges from 0.0573 to 0.1039 m, highlighting minimal average prediction errors. Fold 4 exhibits slightly higher errors, likely as a result of outlier or extreme collected data. Overall, the low dispersion of R^2 and MAE supports the model's robustness and stability. Table 5 presents the results obtained for this case.

Table 5. Cross-validation performance metrics of the MLP model using ReLU activation

Fold	R^2	RMSE (m)	MAE (m)
1	0.9927	0.0879	0.0573
2	0.9843	0.1362	0.0722
3	0.9851	0.1249	0.0904
4	0.9628	0.1934	0.1039
5	0.9843	0.1159	0.0776
6	0.9805	0.1227	0.0720

The results confirm that MLP-RELU accurately simulates the functional relationship between dam structural characteristics (height, length, density, elastic modulus) and extreme horizontal displacement, ensuring reliable insights into the dam's structural behavior under loading.

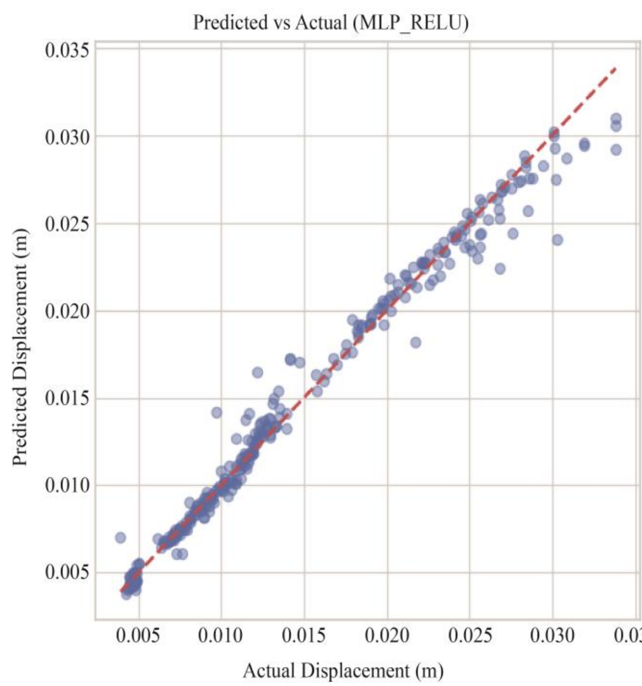

Fig. 9 Predicted vs Actual Displacement for MLP Model using ReLU Activation

As illustrated in the figure 9, the data points are closely aligned along the diagonal line, demonstrating high precision and low dispersion in predictions of maximum displacement by the MLP model with ReLU activation.

4.2.2. MLP with Tanh Activation

The MLP model using Tanh activation shows reliably high predictive capability among six-fold cross-validation, with R^2 values between 0.9848 and 0.9926. RMSE varies from 0.0879 to 0.1341 m, and MAE from 0.0573 to 0.0788 m, demonstrating low average model errors. Table 6 presents the results obtained for this case.

Table 6. Cross-validation performance metrics of the MLP model using Tanh activation

Fold	R^2	RMSE (m)	MAE (m)
1	0.9922	0.0912	0.0591
2	0.9848	0.1341	0.0788
3	0.9926	0.0879	0.0573
4	0.9877	0.1114	0.0710
5	0.9887	0.0983	0.0715
6	0.9888	0.0931	0.0592

In general, MLP-Tanh accurately captures the correlation between dam geometrical-mechanical properties and maximal horizontal displacement, providing reliable and precise structural predictions.

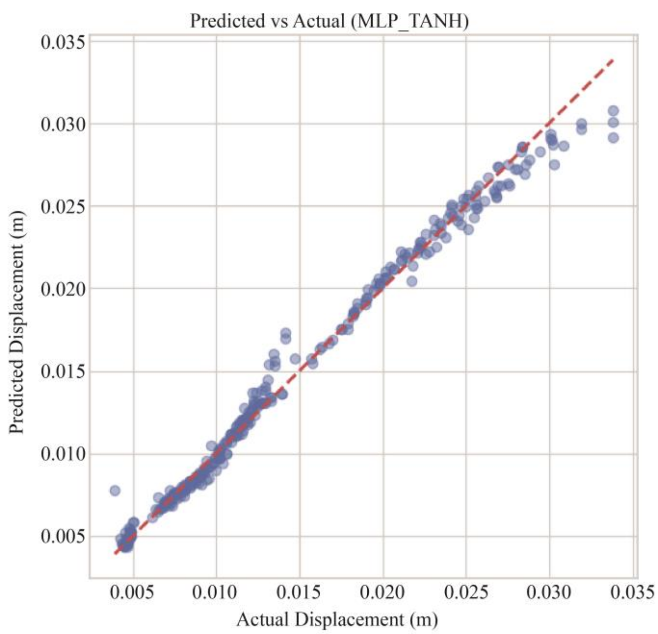

Fig. 10 Predicted vs Actual Displacement for MLP Model using Tanh Activation

As illustrated in the figure 10, the MLP-Tanh predictions closely follow the actual measurements, reflecting the model's reliability and stable performance across different validation sets.

4.2.3. MPL with Logistic Activation

The MLP model with Logistic activation exhibits limited predictive performance, with R^2 values ranging between 0.5560 and 0.7439. RMSE lies between 0.4497 and 0.6682 m, and MAE between 0.3095 and 0.4883 m, indicating higher prediction errors compared to the results of the same model with Relu and Tanh activations. Table 7 presents the results obtained for this case.

Table 7. Cross-validation performance metrics of the MLP model using logistic activation

Fold	R^2	RMSE (m)	MAE (m)
1	0.7439	0.5215	0.4009
2	0.6852	0.6095	0.4468
3	0.7186	0.5425	0.4133
4	0.5560	0.6682	0.4883
5	0.5731	0.6050	0.4580
6	0.7386	0.4497	0.3095

The larger variability across the validation folds reflects lower model stability. This suggests that the MLP architecture with logistic activation struggles to model the nonlinear relationship between dam geometrical and structural features and maximal horizontal displacement under hydraulic and seismic loads.

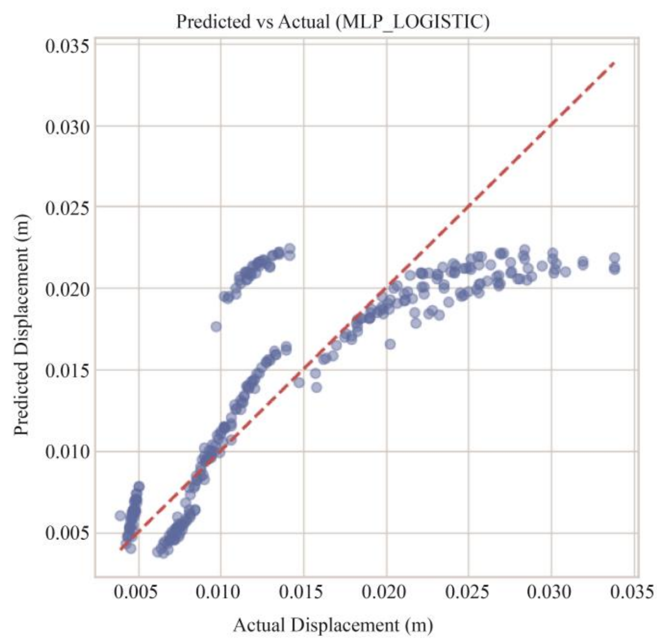

Fig. 11 Predicted vs Actual Displacement for MLP Model using Logistic Activation

As presented in Figure 11, the MLP-Logistic model demonstrates greater dispersion around the diagonal, reflecting reduced predictive capability, especially for the extreme observations observed in fold 4 and 5.

The comparative evaluation of different MLP models confirms that the choice of activation function highly affects predictive accuracy. MLPs with Relu and Tanh activations achieved the greatest performance, with mean R^2 values exceeding 0.98, indicating excellent performance to capture the variance of maximum dam displacements. These models also presented low variability across validation folds, demonstrating reliability and stability against fluctuations in test set results. In contrast, the Logistic activation exhibited considerably lower performance, with mean R^2 close to 0.67 and higher errors, revealing its limited capability to capture complex nonlinear relationships among mechanical and geometrical properties.

4.3. Support Vector Regression (SVR) Model Performance
4.3.1. SVR with RBF Kernel

The simulation results indicate that the SVR model with RBF kernel exhibits higher predictive capability, with R^2 extending from 0.9866 to 0.9946. A very low RMSE ranging from 0.0683 to 0.1184 m, and MAE between 0.0348 and 0.0665 m, highlighting accurate predictions across all validation folds. Limited dispersion of metrics confirms high stability. Table 8 presents the obtained results.

Table 8. Cross-validation performance metrics of the SVR model with RBF kernel

Fold	R^2	RMSE (m)	MAE (m)
1	0.9940	0.0795	0.0348
2	0.9900	0.1088	0.0504
3	0.9866	0.1184	0.0665
4	0.9918	0.0907	0.0461
5	0.9946	0.0683	0.0354
6	0.9901	0.0874	0.0516

The RBF kernel effectively models nonlinear relationships across dam structural and geometrical features, accurately predicting maximal horizontal displacement under applied loads.

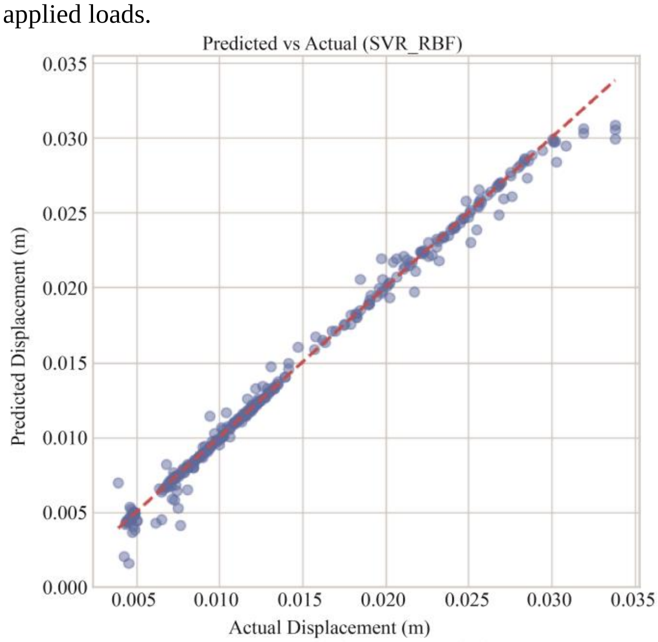

Fig. 12 Predicted vs actual displacement for the SVR model with RBF kernel

As illustrated in Figure 12, SVR with RBF kernel exhibits strong correlation between predicted and actual displacements, highlighting its capability to capture non-linear interactions effectively.

4.3.2. SVR with Linear Kernel

Respectively, the SVR model with a linear kernel demonstrates moderate predictive performance, with R^2 values ranging from 0.4883 to 0.7427. A high RMSE and MAE (0.5060–0.7173 m and 0.3189–0.5018 m), highlighting moderate ability to capture nonlinear relationships. Table 9 presents the results obtained for this case.

Table 9. Cross-validation performance metrics of the SVR model with linear kernel

Fold	R^2	RMSE (m)	MAE (m)
1	0.7418	0.5236	0.3781
2	0.7015	0.5935	0.3979
3	0.7427	0.5188	0.3401
4	0.4883	0.7173	0.5018
5	0.5049	0.6515	0.4624
6	0.6690	0.5060	0.3189

The performance variability among validation folds indicates that linear assumptions in SVR method are insufficient to model the complex mechanical behavior of the dam under loads.

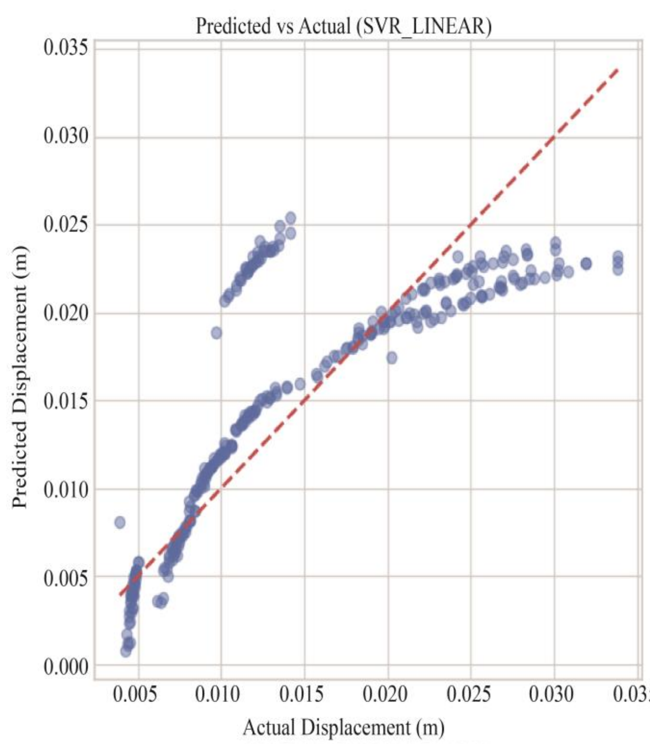

Fig. 13 Predicted vs actual displacement for the SVR Model with linear kernel

The figure 13 illustrates that the linear kernel models the overall trend but exhibits larger dispersions for some extreme observations, highlighting limitations in capturing non-linear interactions and prediction performance.

4.3.3. SVR with Polynomial Kernel

The application of SVR model with a polynomial kernel indicates unstable performance, with R^2 ranging from 0.4789 to 0.7020. Hight RMSE varies between 0.4963 to 0.7120 m, and considerable MAE between 0.3185 and 0.5079 m. Table 10 presents the results obtained for this case.

Table 10. Cross-validation performance metrics of the SVR model with polynomial kernel

Fold	R^2	RMSE (m)	MAE (m)
1	0.5225	0.7120	0.5079
2	0.7020	0.5930	0.3408
3	0.5315	0.7000	0.4739
4	0.5483	0.6740	0.4836
5	0.4789	0.6684	0.4801
6	0.6817	0.4963	0.3185

These results demonstrate sensitivity to data heterogeneity and some limitations in capturing complex relationships for dam's dynamical behavior.

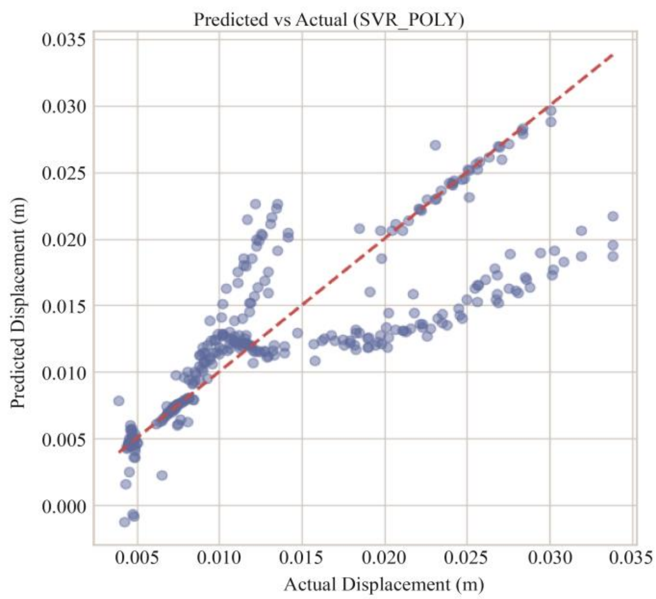

Fig. 14 Predicted vs actual displacement for the SVR model using polynomial kernel

As illustrated in Figure 14, the polynomial kernel exhibits intermediate efficiency, with moderate dispersion suggesting partial modeling of the problem's complexity.

The findings indicate that the SVR models with different kernel functions reveals substantial differences in predictive performance. The RBF kernel systematically outperformed linear and polynomial kernels, indicating its greatest capability to capture nonlinear complexity in dam mechanical behavior under loads. In contrast, the Linear kernel demonstrated moderate performance, highlighting limitations in modeling nonlinear interactions. The Polynomial kernel showed the lowest stability and predictive accuracy, with R^2 under 0.55 for some folds and higher error values, assuming sensitivity to data heterogeneity and complexity. Overall, the results demonstrate that SVR with RBF kernel is best suitable for modeling the maximum horizontal displacement of dams, while linear and polynomial kernels are less reliable for capturing the nonlinear mechanical and geometrical features.

4.4. Extreme Gradient Boosting XGBoost Model Performance

4.4.1. Extreme Gradient Boosting XGBoost Model

The XGBoost model demonstrates exceptional predictive performance across all six validation folds. The coefficient of determination (R^2) varies from 0.9944 to 0.9981, indicating that the model effectively captures almost all the variance within the displacement data. The RMSE is consistently low, between 0.0449 and 0.0774 m, reflecting marginal deviations between predicted and measured values. Similarly, the mean absolute error (MAE) ranges from 0.0258 m to 0.0344 m, exhibiting high prediction accuracy. Table 11 presents the obtained results for this case.

Table 11. Cross-validation performance metrics of the XGBoost model

Fold	R^2	RMSE (m)	MAE (m)
1	0.9944	0.0774	0.0344
2	0.9976	0.0528	0.0307
3	0.9981	0.0449	0.0278
4	0.9975	0.0500	0.0259
5	0.9973	0.0481	0.0269
6	0.9974	0.0449	0.0258

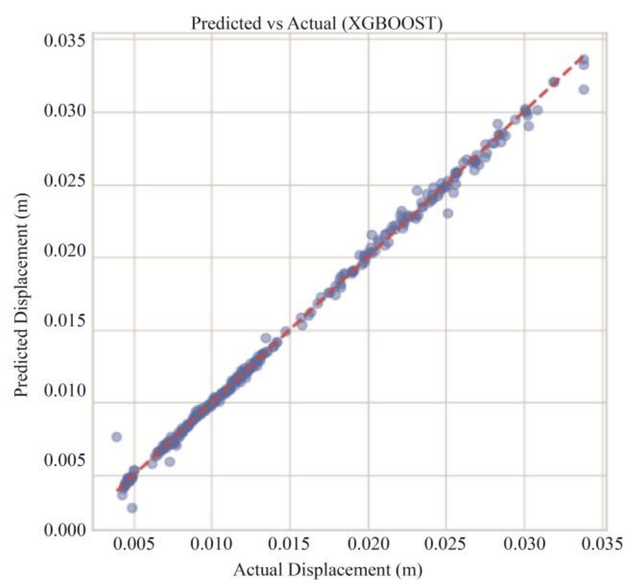

Fig. 15 Predicted vs actual displacement for the XGBoost model

The limited dispersion of errors across the different folds highlights the robustness and stability of XGBoost. Generally, these results indicate that XGBoost effectively captures the nonlinear interactions between the geometrical-mechanical features of the dam and the maximum horizontal displacement under hydraulic and seismic loads, outperforming linear regression models and demonstrating greater reliability for structural behavior prediction of dams' maximal displacement.

As illustrated in Figure 15, XGBoost model predictions align almost perfectly with actual observed values, confirming superior accuracy and robustness for this dataset. The comparison between MLP, SVR, and XGBoost models indicates that all methods capture the relationship between dam properties and maximum displacement under hydraulic and seismics loads. MLP with Relu and Tanh activations ensures higher performance with R^2 exceeding 0.96, while Logistic activation exhibits lower performance. SVR with RBF kernel achieves excellent accuracy with R^2 greater than 0.98, and negligible error, outperforming Linear and Polynomial kernels. XGBoost provides the highest performance, with R^2 exceeding 0.994.

Overall, XGBoost represents the most accurate and recommended model for reliable dam maximal displacement prediction. MLP and SVR remain effective with competitive accuracy, ensuring practical alternatives in dam engineering applications. Table 12 presents the Comparative Summary of All Models used in this study.

Table 12. Comparative summary of all models based on average cross-validation metrics

Model	R^2 Mean	R^2 Std	RMSE Mean (m)	RMSE Std	MAE Mean (m)	MAE Std
MLP_RELU	0.9849	0.0097	0.1303	0.0378	0.0725	0.0150
MLP_TANH	0.9908	0.0035	0.1026	0.0177	0.0663	0.0102
MLP_LOGISTIC	0.6692	0.0654	0.5570	0.0805	0.4351	0.0556
SVR_RBF	0.9912	0.0027	0.0922	0.0169	0.0475	0.0108
SVR_LINEAR	0.6414	0.1055	0.5851	0.0779	0.3999	0.0644
SVR_POLY	0.5775	0.0837	0.6406	0.0749	0.4341	0.0749
XGBoost	0.9977	0.0017	0.0465	0.0115	0.0303	0.0038

The Figures 16-17 bellow illustrate the results previously discussed. XGBoost and MLP-ReLU/Tanh achieve the highest R^2 and the lowest RMSE and MAE, demonstrating superior accuracy in predicting dam displacement.

In contrast, lower R^2 values for MLP-Logistic and SVR-Polynomial suggesting reduced capture of nonlinear relationships, especially in dam displacement prediction.

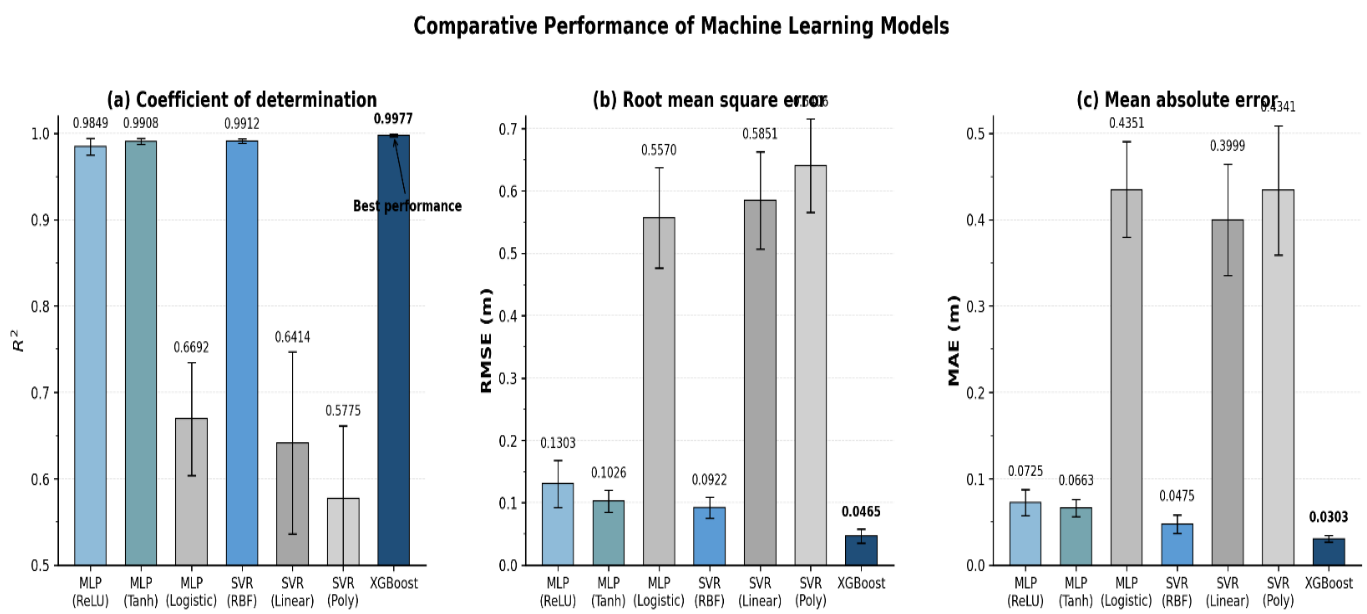

Fig. 16 Comparative performance of the evaluated machine learning models based on R^2, RMSE, and MAE

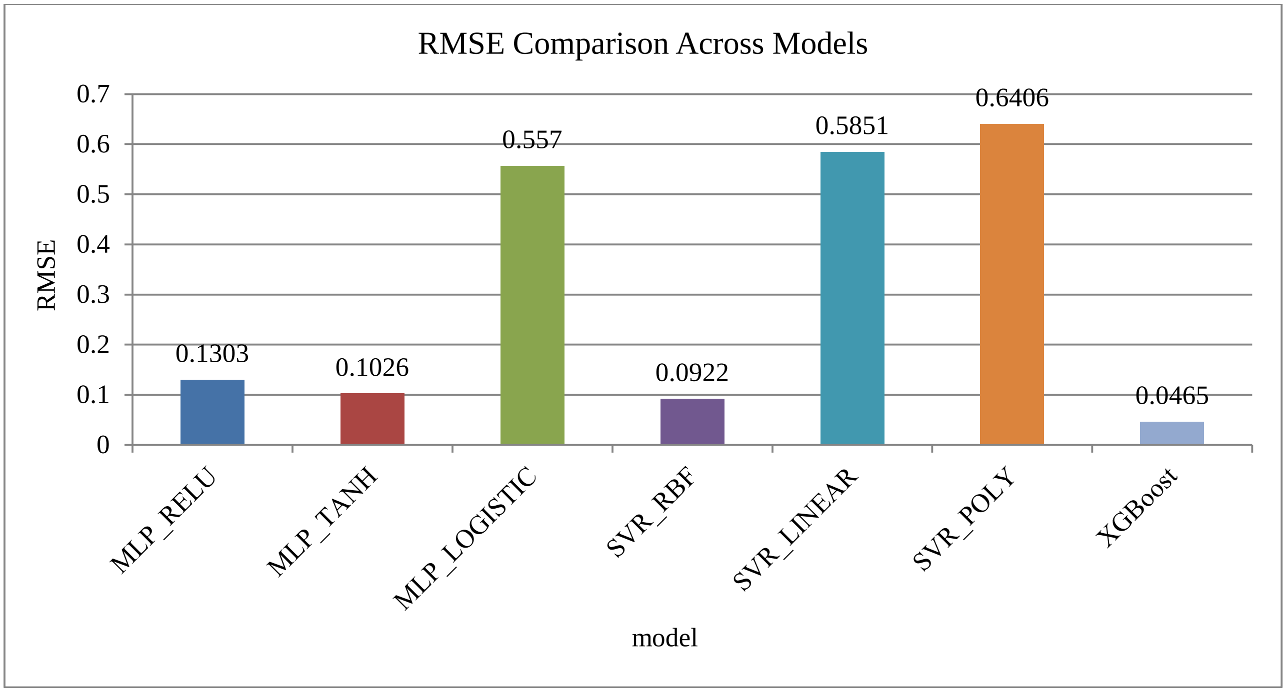

Fig. 17 Comparison of RMSE across all models

4.5. Hyperparameter optimization of ML Models

4.5.1. Hyperparameter Optimization of MLP Model

The hyperparameter optimization process of MLP model identified a neural network architecture composed of two hidden layers with 64 and 32 neurons as the optimal configuration for seismic displacement prediction. Indeed, the tanh activation function outperformed the other tested activation functions, indicating its capability to effectively capture the complex nonlinear relationships between the input features and the output variable. Furthermore, the optimal learning rate was found to be 0.01, suggesting that a moderate learning rate provided the best balance between convergence speed and predictive accuracy. Table 13 summarizes the optimal hyperparameter configuration obtained for the MLP model through the Grid Search optimization process.

Table 13. Optimal hyperparameter configuration of the MLP model

Hyperparameter	Tested Values	Optimal Value
Hidden Layer Architecture	(32,), (64,), (128,), (32,16), (64,32), (128,64)	(64, 32)
Activation Function	Relu, tanh, logistic	tanh
Learning Rate	0.0001, 0.001, 0.01	0.01

Following hyperparameter optimization, the model was evaluated using six-fold cross-validation to assess its predictive performance and generalization ability. Table 14 reports the obtained R², RMSE, and MAE values across the six validation folds applied to the best MLP configuration.

Table 14. Cross-validation performance metrics of the MLP model using the optimized values

Fold	R^2	RMSE (m)	MAE (m)
1	0.9948	0.000596	0.000244
2	0.9962	0.000517	0.000271
3	0.9958	0.000520	0.000297
4	0.9985	0.000287	0.000211
5	0.9967	0.000431	0.000259
6	0.9968	0.000418	0.000340

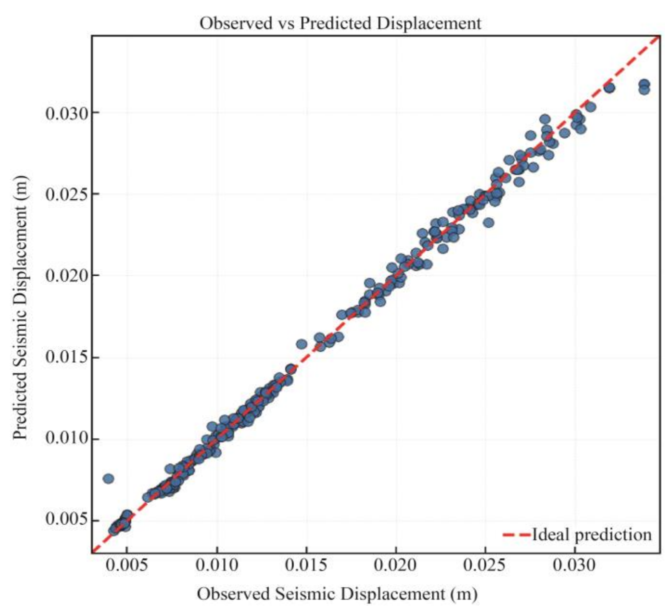

Fig. 18 Predicted vs. Observed displacement for the optimized MLP Model

The MLP model consistently exhibited excellent predictive capability across the six validation folds, with R^2 values ranging from 0.9948 to 0.9985, indicating a very high degree of agreement between the predicted and observed seismic displacements. Figure 18 illustrates the correlation between the predicted and observed seismic displacements.

4.5.2. Hyperparameter optimization of SVR model

The Grid Search optimization procedure identified the optimal Linear SVR configuration as C = 1 and ε = 0.001, resulting in a mean cross-validation R^2 score of 0.6319. Similarly, the optimal Polynomial SVR model was identified with C = 100, degree = 4, ε = 0.001, and gamma = scale, achieving a mean cross-validation R^2 score of 0.5983. Among the evaluated kernels, the RBF-SVR model achieved the best performance with C = 10, γ = scale, and ε = 0.001, yielding the highest cross-validation R^2 score of 0.9736. These results demonstrate the superior ability of the RBF kernel to capture the nonlinear relationship between the input variables and the seismic displacement response, outperforming both the Linear and Polynomial kernels. Table 15 summarizes the SVR hyperparameter values explored during the Grid Search optimization.

Table 15. Comparative hyperparameter optimization results of the SVR kernels

Kernel	Candidate Values	Optimal Hyperparameter
Linear	C {0.1, 1, 10, 100}	C = 1
	ε{0.001, 0.01, 0.1}	ε = 0.001
Polynomial	C {0.1, 1, 10, 100}	C = 100
	ε{0.001, 0.01, 0.1}	ε = 0.001
	Degree {2, 3, 4}	degree = 4
	γ {scale, auto}	γ = scale
RBF	C {0.1, 1, 10, 100}	C = 10
	ε{0.001, 0.01, 0.1}	ε = 0.001
	γ{0.01, 0.1, 1, scale}	γ = 0.1

The comparative results presented in Table 16 indicate that the RBF kernel consistently achieved the highest predictive performance, with a mean cross-validation R^2 of 0.9736 and considerably lower RMSE and MAE values than the Linear and Polynomial kernels. Based on its superior predictive performance, the RBF-SVR model was selected for further evaluation and detailed analysis.

Table 16. Comparative performance of SVR kernels

Kernel	R^2	RMSE (m)	MAE (m)
Linear	0.6319	0.004618	0.003216
Polynomial	0.5983	0.004954	0.003395
RBF	0.9736	0.001245	0.000959

Following the kernel comparison, the optimized RBF-SVR model was evaluated using six-fold cross-validation to assess its predictive performance and generalization ability. Table 17 reports the R^2, RMSE, and MAE values obtained across the six cross-validation folds.

Table 17. Cross-validation performance metrics of the RBF-SVR Model using the optimized values

Fold	R^2	RMSE (m)	MAE (m)
1	0.9846	0.001026	0.000814
2	0.9668	0.001534	0.001190
3	0.9790	0.001165	0.000919
4	0.9819	0.000985	0.000779
5	0.9778	0.001118	0.000942
6	0.9513	0.001642	0.001111

The optimized RBF-SVR model consistently achieved high predictive performance throughout the six validation folds, with R^2 values varying between 0.9513 and 0.9846. Moreover, the limited variability in the performance metrics demonstrates good robustness and generalization ability.

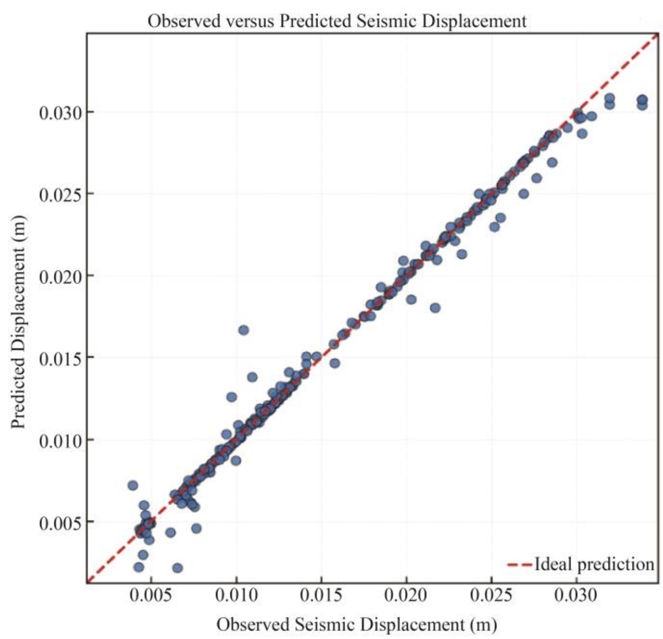

Fig. 19 Predicted vs. Observed displacement for the optimized RBF-SVR model

As seen in Figure 19, the predicted values closely follow the observed data and remain close to the identity line, confirming the satisfactory predictive performance and explaining approximately 97% of the variability in seismic displacement.

4.5.3. Hyperparameter optimization of XGBoost model

The optimal XGBoost configuration consisted of 300 trees, a maximum depth of 4 and a learning rate of 0.05, achieving a mean cross-validation R^2 value of 0.9961. Table 18 presents the hyperparameter values explored to identify the optimal model configuration.

Table 18. Comparative hyperparameter optimization results of the XGBoost model

Hyperparameter	Tested Values	Optimal Value
N_estimators	100, 200, 300	300
Max_depth	2, 3, 4, 5, 6	4
Learning_rate	0.01, 0.05, 0.1	0.05
Subsample	0.7, 0.8, 1.0	0.7
Colsample_bytree	0.7, 0.8, 1.0	1.0

After the hyperparameter optimization, the optimized XGBoost model was evaluated using six-fold cross-validation to assess its predictive performance. The resulting R^2, RMSE, and MAE values are presented in Table 19.

Table 19. Cross-validation performance metrics of XGBoost model using the optimized values

Fold	R^2	RMSE (m)	MAE (m)
1	0.9946	0.000608	0.000294
2	0.9949	0.000600	0.000346
3	0.9955	0.000539	0.000346
4	0.9968	0.000416	0.000268
5	0.9978	0.000348	0.000267
6	0.9969	0.000415	0.000306

The optimized XGBoost model achieved excellent predictive performance across all six cross-validation folds, with R^2 values ranged from 0.9946 to 0.9978 and consistently low RMSE and MAE values, confirming the stability and robustness of the model.

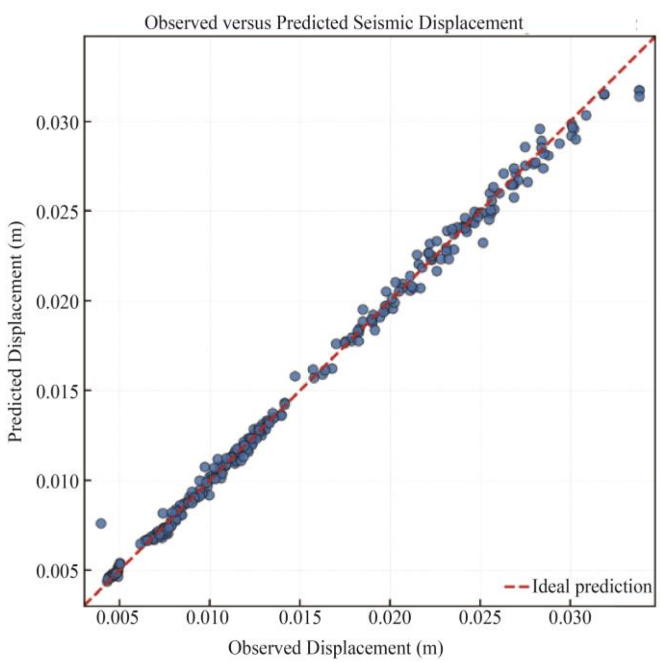

Fig. 20 Predicted versus observed values for the XGBoost optimized model

As illustrated in Figure 20, the predicted values are closely aligned with the observed data and are concentrated around the identity line, demonstrating excellent model performance.

4.6. Comparative Performance Assessment of ML Models

The comparative results indicate that both MLP and XGBoost models achieved excellent predictive performance, with mean R^2 values exceeding 0.996 and very low prediction errors. Although the performance difference between the two models was relatively small, the MLP consistently demonstrated slightly higher predictive accuracy across the six cross-validation folds. In contrast, RBF-SVR model exhibited lower predictive performance, with a mean R^2 of 0.9736 and noticeably higher error values, as summarized in Table 20.

Table 20. Comparative predictive performance of the evaluated models

Model	Mean R^2	Mean RSME (m)	Mean MAE (m)
MLP	0.9965	0.000462	0.000270
SVR	0.9736	0.001245	0.000959
XGBoost	0.9961	0.000488	0.000305

These findings demonstrate the superior predictive performance of the MLP model in capturing the complex nonlinear relationships between the input variables and the maximum seismic displacement. Figure 21 illustrates the comparative predictive performance of the three machine learning models.

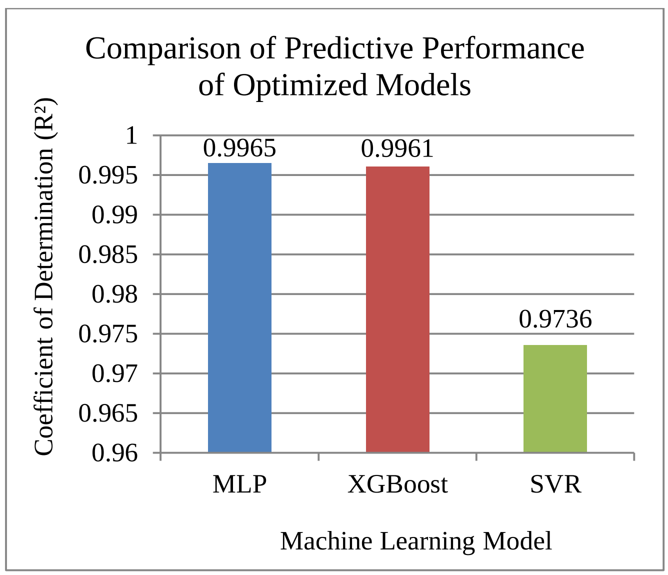

Fig. 21 Comparison of cross-validation R^2 scores of the evaluated models

4.7. Feature Importance Analysis

Despite the MLP model achieved the highest predictive accuracy with an R^2 of 0.996, the XGBoost model demonstrated a very similar performance (R^2 = 0.9961).

Therefore, the XGBoost model was selected for the interpretability analysis because it achieved the best predictive performance and provides an inherently interpretable mechanism for quantifying the relative contribution of each input variable, comparable to the optimal MLP model.

The feature importance analysis reveals the predominant influence of dam height on seismic displacement prediction, accounting for 94.53% of the total importance. Elastic modulus ranked second with 3.64%, followed by dam length (1.39%) and density (0.42%). The corresponding importance scores are illustrated in Figure 22. These findings indicate that the seismic response is predominantly influenced by the geometric characteristics of the dam, particularly its height.

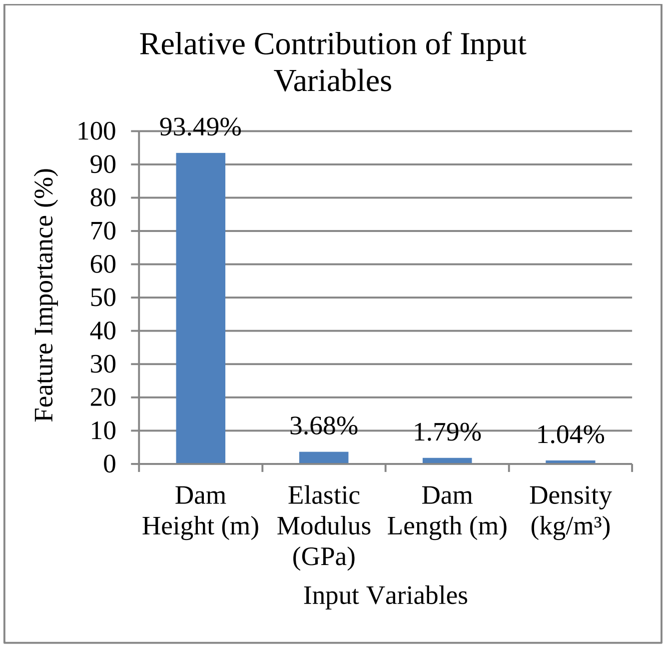

Fig. 22 Feature importance derived from the optimized XGBoost model for maximum dam displacement prediction

4.8. Sensitivity and Robustness Analysis

To evaluate the robustness and reliability of the developed XGBoost model, a perturbation-based sensitivity analysis was conducted. Indeed, each input variable was independently perturbed by increasing its value by 1%, 3%, 5%, and 7% across all observations, while the remaining input variables remained unchanged.

Moreover, the trained model was subsequently applied on the perturbed datasets, and the resulting variations in prediction performance were quantified using the coefficient of determination (R^2). The corresponding results are summarized in Figure 23 using a sensitivity heatmap. The sensitivity analysis demonstrates that the predictive performance of the XGBoost model is highly influenced by variations in dam height. This variable exhibits the largest mean absolute variation in R^2 (Mean $|\Delta R^2|$ = 0.42813). In contrast, the elastic modulus exhibited a limited effect (Mean $|\Delta R^2|$ = 0.00194), while density and dam length produced negligible influences, with Mean $|\Delta R^2|$ values close to zero. These findings further confirm that dam height is the dominant controlling factor governing the predicted displacement response.

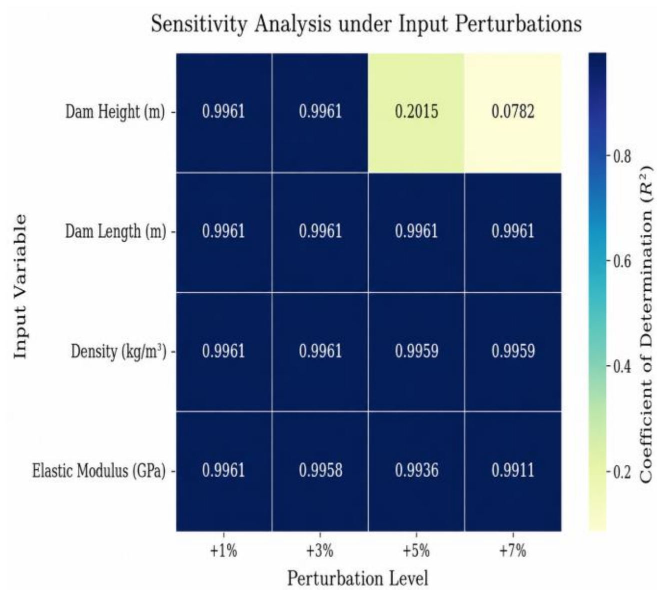

Fig. 23 Sensitivity Heatmap of R^2 values under input perturbations

Despite exhibiting the highest sensitivity to perturbations in dam height, the XGBoost model maintained high predictive performance, demonstrating satisfactory robustness. Overall, the results indicate that strong agreement was observed between the SHAP-based feature importance and the sensitivity and robustness analysis, both highlighting dam height as the most influential variable.

5. Conclusion

The present study developed and evaluated the capability of machine learning techniques for predicting the maximum seismic displacement of concrete gravity dams within an SDOF-based seismic reliability context. A comprehensive dataset was generated through finite element simulations covering a representative range of geometric and material properties of the dam system.

Moreover, a comparative assessment of MLP, SVR, and XGBoost models demonstrated the superior predictive capability of the MLP model, while XGBoost achieved nearly identical predictive performance with only marginal differences in accuracy and error metrics. Furthermore, The SHAP and sensitivity analyses consistently identified dam height as the dominant factor governing the predicted seismic response, whereas the remaining input variables exhibited comparatively limited influence within the investigated parameter range. Finally, although the proposed models demonstrated high predictive accuracy, their performance remains inherently dependent on the quality and representativeness of the training dataset. The present study was limited to a specific range of geometric and material properties, which may constrain the generalizability of the proposed models to other concrete gravity dam configurations or seismic loading conditions. Future research could extend the proposed framework by incorporating larger datasets and additional physical parameters to further improve both predictive performance and model interpretability.

References

[1] Giacomo Sevieri, and Anna De Falco, "Dynamic Structural Health Monitoring for Concrete Gravity Dams based on the Bayesian Inference," *Journal of Civil Structural Health Monitoring*, vol. 10, no. 2, pp. 235-250, 2020. [CrossRef] [Google Scholar] [Publisher Link]

[2] Shuyang Yu et al., "Seepage, Deformation, and Stability Analysis of Sandy and Clay Slopes with Different Permeability Anisotropy Characteristics Affected by Reservoir Water Level Fluctuations," *Water*, vol. 12, no. 1, pp. 1-20, 2020. [CrossRef] [Google Scholar] [Publisher Link]

[3] Sihan Song et al., "Automatic Concrete Dam Deformation Prediction Model Based on TPE-STL-LSTM," *Water*, vol. 15, no. 11, pp. 1-48, 2023. [CrossRef] [Google Scholar] [Publisher Link]

[4] Jiedeerbieke Madiniyeti et al., "Concrete Dam Deformation Prediction Model Research Based on SSA–LSTM," *Applied Sciences*, vol. 13, no. 13, pp. 1-15, 2023. [CrossRef] [Google Scholar] [Publisher Link]

[5] Neander Berto Mendes, and Lineu José Pedroso, "Structural Verification of a Gravity Dam under Seismic Action using Machine Learning," *Computers & Structures*, vol. 321, 2026. [CrossRef] [Google Scholar] [Publisher Link]

[6] Chuan Lin et al., "Variation Trend Prediction of Dam Displacement in the Short-Term Using a Hybrid Model Based on Clustering Methods," *Applied Sciences*, vol. 13, no. 19, pp. 1-24, 2023. [CrossRef] [Google Scholar] [Publisher Link]

[7] Wenyuan Wu et al., "A Novel Artificial Intelligence Prediction Process of Concrete Dam Deformation Based on a Stacking Model Fusion Method," *Water*, vol. 16, no. 13, pp. 1-26, 2024. [CrossRef] [Google Scholar] [Publisher Link]

[8] Thanh T. Nguyen et al., "Influence of Settlement on Base Resistance of Long Piles in Soft Soil—Field and Machine Learning Assessments," *Geotechnics*, vol. 4, no. 2, pp. 447-469, 2024. [CrossRef] [Google Scholar] [Publisher Link]

[9] Yan Su et al., "Dam Deformation Monitoring Model Based on Deep Learning and Split Conformal Quantile Prediction," *Applied Sciences*, vol. 15, no. 4, pp. 1-18, 2025. [CrossRef] [Google Scholar] [Publisher Link]

[10] Yaren Aydın et al., "Explainable Ensemble Learning and Multilayer Perceptron Modeling for Compressive Strength Prediction of Ultra-High-Performance Concrete," *Biomimetics*, vol. 9, no. 5, pp. 1-15, 2024. [CrossRef] [Google Scholar] [Publisher Link]

[11] Ezgi Gurgenc, Osman Altay, and Elif Varol Altay, "AOSMA-MLP: A Novel Method for Hybrid Metaheuristics Artificial Neural Networks and a New Approach for Prediction of Geothermal Reservoir Temperature," *Applied Sciences*, vol. 14, no. 8, pp. 1-19, 2024. [CrossRef] [Google Scholar] [Publisher Link]

[12] Husam Ahmad Al Hamada, and Mohammad Shehab, "Integrated Multi-Layer Perceptron Neural Network and Novel Feature Extraction for Handwritten Arabic Recognition," *International Journal of Data and Network Science*, vol. 8, no. 3, pp. 1501-1516, 2024. [CrossRef] [Google Scholar] [Publisher Link]

[13] Wendi Jia, and Quanlong Chen, "Aircraft Structural Stress Prediction Based on Multilayer Perceptron Neural Network," *Applied Sciences*, vol. 14, no. 21, pp. 1-21, 2024. [CrossRef] [Google Scholar] [Publisher Link]

[14] Mintae Kim et al., "Deep Learning Approach on Prediction of Soil Consolidation Characteristics," *Buildings*, vol. 14, no. 2, pp. 1-18, 2024. [CrossRef] [Google Scholar] [Publisher Link]

[15] Andrés Mauricio Guzmán Sejas et al., "Developing Statistical and Multilayer Perceptron Neural Network Models for a Concrete Dam Dynamic Behaviour Interpretation," *Infrastructures*, vol. 10, no. 11, pp. 1-17, 2025. [CrossRef] [Google Scholar] [Publisher Link]

[16] Younes Alouan et al., "Multi-Layer Perceptron Neural Networks for Concrete Strength Prediction: Balancing Performance and Optimizing Mix Designs," *Engineering Proceedings*, vol. 112, no. 1, pp. 1-11, 2025. [CrossRef] [Google Scholar] [Publisher Link]

[17] You-Jeng Chang, Ying-Lei Lin, and Ping-Feng Pai, "Support Vector Machines with Hyperparameter Optimization Frameworks for Classifying Mobile Phone Prices in Multi-Class," *Electronics*, vol. 14, no. 11, pp. 1-21, 2025. [CrossRef] [Google Scholar] [Publisher Link]

[18] Jonatha Sousa Pimentel, Raydonal Ospina, and Anderson Ara, "A Novel Fusion Support Vector Machine Integrating Weak and Sphere Models for Classification Challenges with Massive Data," *Decision Analytics Journal*, vol. 11, pp. 1-14, 2024. [CrossRef] [Google Scholar] [Publisher Link]

[19] Rosita Guido et al., "An Overview on the Advancements of Support Vector Machine Models in Healthcare Applications: A Review," *Information*, vol. 15, no. 4, pp. 1-36, 2024. [CrossRef] [Google Scholar] [Publisher Link]

[20] Ehsan Harirchian et al., "Application of Support Vector Machine Modeling for the Rapid Seismic Hazard Safety Evaluation of Existing Buildings," *Energies*, vol. 13, no. 13, pp. 1-15, 2020. [CrossRef] [Google Scholar] [Publisher Link]

[21] Wei Shao et al., “The Application of Machine Learning Techniques in Geotechnical Engineering: A Review and Comparison,” *Mathematics*, vol. 11, no. 18, pp. 1-16, 2023. [CrossRef] [Google Scholar] [Publisher Link]

[22] Saurabh Kumar Anuragi, “Application of Support Vector Machine in Geotechnical Engineering: A Review,” *Global Journal of Engineering and Technology Advances*, vol. 21, no. 3, pp. 103-113, 2024. [CrossRef] [Google Scholar] [Publisher Link]

[23] Xin Yang, Yan Xiang, Guangze Shen, and Meng Sun, “A Combination Model for Displacement Interval Prediction of Concrete Dams Based on Residual Estimation,” *Sustainability*, vol. 14, no. 23, pp. 1-17, 2022. [CrossRef] [Google Scholar] [Publisher Link]

[24] Asif Ahmed et al., “Hybrid BO-XGBoost and BO-RF Models for the Strength Prediction of Self-Compacting Mortars with Parametric Analysis,” *Materials*, vol. 16, no. 12, pp. 1-27, 2023. [CrossRef] [Google Scholar] [Publisher Link]

[25] Billal Sari-Ahmed et al., “Strength Prediction of Fiber-Reinforced Clay Soils Stabilized with Lime Using XGBoost Machine Learning,” *Civil and Environmental Engineering Reports*, vol. 34, no. 2, pp. 157-176, 2024. [CrossRef] [Google Scholar] [Publisher Link]

[26] Duygu Demirtürk, Ömer Mintemur, and Abdussamet Arslan, “Optimizing LightGBM and XGBoost Algorithms for Estimating Compressive Strength in High-Performance Concrete,” *Arabian Journal for Science and Engineering*, vol. 51, no. 4, pp. 4401-4423, 2026. [CrossRef] [Google Scholar] [Publisher Link]

[27] Juli Sergine Tavares Teixeira Saldanha et al., “A Comparison of WaveNet and XGBoost for Traditional Direct Wave Propagation and Seismic Inversion using Horizontal Layer Models,” *Research, Society and Development*, vol. 13, no. 5, pp. 1-17, 2024. [CrossRef] [Google Scholar] [Publisher Link]

[28] Nazmus Sakib Ahmed, “Machine Learning Models for Pavement Structural Condition Prediction: A Comparative Study of Random Forest (RF) and eXtreme Gradient Boosting (XGBoost),” *Open Journal of Civil Engineering*, vol. 14, no. 4, pp. 570-586, 2024. [CrossRef] [Google Scholar] [Publisher Link]

[29] Yingui Qiu et al., “Developing Hybrid XGBoost Model to Predict the Strength of Polypropylene and Straw Fibers Reinforced Cemented Paste Backfill and Interpretability Insights,” *CMES - Computer Modeling in Engineering and Sciences*, vol. 144, no. 2, pp. 1607-1629, 2025. [CrossRef] [Google Scholar] [Publisher Link]

[30] Suraj Kumar Parhi, and Sanjaya Kumar Patro, “Prediction of Compressive Strength of Geopolymer Concrete using a Hybrid Ensemble of Grey Wolf Optimized Machine Learning Estimators,” *Journal of Building Engineering*, vol. 71, 2023. [CrossRef] [Google Scholar] [Publisher Link]

[31] Odey Alshboul et al., “Extreme Gradient Boosting-Based Machine Learning Approach for Green Building Cost Prediction,” *Sustainability*, vol. 14, no. 11, pp. 1-20, 2022. [CrossRef] [Google Scholar] [Publisher Link]

[32] Qiubing Ren et al., “A Multiple-Point Monitoring Model for Concrete Dam Displacements based on Correlated Multiple-Output Support Vector Regression,” *Structural Health Monitoring*, vol. 21, no. 6, pp. 2768-2785, 2022. [CrossRef] [Google Scholar] [Publisher Link]

[33] Chongshi Gu et al., “Multi-Output Displacement Health Monitoring Model for Concrete Gravity Dam in Severely Cold Region based on Clustering of Measured dam Temperature Field,” *Structural Health Monitoring*, vol. 22, no. 5, pp. 3416-3436, 2023. [CrossRef] [Google Scholar] [Publisher Link]

[34] Bo Xu et al., “A Deep Learning Prediction and Interpretation Method for Concrete Dam Displacement Considering the Lag Effect and the Impact of Cracks,” *Engineering Research Express*, vol. 7, no. 2, 2025. [CrossRef] [Google Scholar] [Publisher Link]

[35] Muhammad Fikri Alam et al., “Optimizing Multi-Layer Perceptron Performance in Sentiment Classification through Neural Network Feature Extraction,” *BACA: Journal of Documentation and Information*, vol. 46, no. 1, pp. 1-14, 2025. [CrossRef] [Google Scholar] [Publisher Link]

[36] Xiang Yu et al., “A Continual-Learning-based Multilayer Perceptron for Improved Reconstruction of Three-dimensional Nitrate Concentrations,” *Earth System Science Data*, vol. 17, no. 6, pp. 2735-2759, 2025. [CrossRef] [Google Scholar] [Publisher Link]

[37] Bandar Alshawi, “Comparison of SVM Kernels in Credit Card Fraud Detection using GANs,” *International Journal of Advanced Computer Science and Applications (IJACSA)*, vol. 15, no. 1, pp. 330-337, 2024. [CrossRef] [Google Scholar] [Publisher Link]

[38] Carlos Aníbal Suárez et al., “Improving SVM Performance through Data Reduction and Misclassification Analysis with Linear Programming,” *Complex & Intelligent Systems*, vol. 11, no. 8, pp. 1-9, 2025. [CrossRef] [Google Scholar] [Publisher Link]

[39] Andrew Oosthuizen, Marelie H. Davel, and Albert Helberg, “Multi-Layer Perceptron for Channel State Information Estimation: Design Considerations,” *Southern Africa Telecommunication Networks and Applications Conference (SATNAC) 2022*, South Africa, pp. 94-99, 2022. [Google Scholar] [Publisher Link]

[40] Yildiran Yilmaz et al., “Predicting Mechanical Properties in Geopolymer Mortars, Including Novel Precursor Combinations, through XGBoost Method,” *Arabian Journal for Science and Engineering*, vol. 50, no. 3, pp. 2009-2033, 2025. [CrossRef] [Google Scholar] [Publisher Link]